THE SENSITIVITY OF SUPERCELL SIMULATIONS TO THE INITIAL CONDITION RESOLUTION

Elisa M. Murillo

National Weather Center Research Experiences for Undergraduates Program, Norman, Oklahoma, and University of Louisiana at Monroe, Monroe, Louisiana

Corey K. Potvin

Cooperative Institute for Mesoscale Meteorological Studies, University of Oklahoma, NOAA/OAR/National Severe Storms Laboratory, and School of Meteorology, University of Oklahoma, Norman, Oklahoma

ABSTRACT

The effects of initial condition resolution on idealized supercell simulations are analyzed. The motivation for this study is based on the NOAA Warn-on-Forecast (WoF) program, which is developing a convention-allowing ensemble system for operational use. The program envisions a paradigm shift from "warn-on-detection," or prediction of severe convective storms based primarily on current observations, to storm-scale data assimilation and prediction systems playing a much greater role in the severe weather warning process. This study focuses on testing the sensitivity of these supercell simulations to the initial condition resolution, which has not yet been systematically studied. Our focus is on the prediction of model quantities of greatest significance to severe storm forecasters, including updraft strength, low-level vorticity, surface winds, and rainfall.

Idealized simulations are run using the WRF-ARW model with grid spacing fixed at 333 m. Each control simulation uses a thermal bubble to initialize a supercell. The model fields from each control simulation are then filtered at various stages of storm development using cutoff wavelengths of 2, 4, 8, and 16 km. New simulations are then initialized from the coarsened model states and compared to the control simulations to assess the impact of the reduced initial condition resolution. Isolating the error due to limited initial condition resolution enables straightforward evaluation of the scales that need to be resolved by data assimilation to generate reliable model forecasts of various severe storm hazards.

Vorticity is the most sensitive out of the model variables analyzed, which can largely impact the tornado potential forecast. Results also indicate that the simulation sensitivity is dependent on the time of initialization. Errors in the simulations initialized early in the storm life cycle do not steadily increase with cutoff wavelength, whereas the simulations initialized once the storm is mature monotonically degrade as filtering is increased. We hypothesize that this is due to smaller scales having a greater impact on storm evolution as the storm develops.

˙1. INTRODUCTION

Due largely to computational limitations, model output currently does not play a major role in short-term, severe storm forecasting. Forecasters are therefore heavily reliant on rapidly changing trends in radar data, often resulting in little warning lead-time for tornadoes, significant hail, damaging winds and flooding. For example, a tornado could already be occurring by the time it is evident in the radar data. This limitation of the current forecasting paradigm, combined with increasing computational capabilities, motivates the development of real-time convection-allowing ensemble modeling systems. The model output would enable the forecaster to issue severe weather warnings with longer lead times. This is the goal of the Warn-on Forecast program (WoF; Strensrud et al. 2009, 2013).

Data assimilation is the process of combining observational data and model output. As WoF continues to make developments, it is important to understand what scales must be resolved by the data assimilation used in model

---

[1] *Corresponding author address:* Elisa Murillo, Department of Atmospheric Science, University of Louisiana at Monroe, 700 University Ave, Monroe, LA, 71209
Email: murillem@warhawks.ulm.edu

initialization. To explore this, we will be testing the sensitivity of supercell simulations to the initial condition resolution. Supercells are the least common type of thunderstorm, yet the most prolific producers of significant hail and tornadoes (hail with 2"+ diameter and tornadoes of EF2+ strength). While this study is focusing on supercell simulations due to their significant hazards, our approach can easily be adapted to other thunderstorm types. In this study, we are varying the initial condition resolution by filtering a high-resolution initial condition using different cutoff wavelengths. Potvin and Flora (2015) used the same method of filtering the initial conditions as in this study; however, their work primarily examined the combined impacts of the initial condition resolution error with the grid resolution error. In one set of experiments, they examined the impact of initial condition resolution alone and found that scales missing from the initial conditions were quickly regenerated during supercell evolution. This study will greatly expand on their preliminary experiments using a range of initialization times and resolutions.
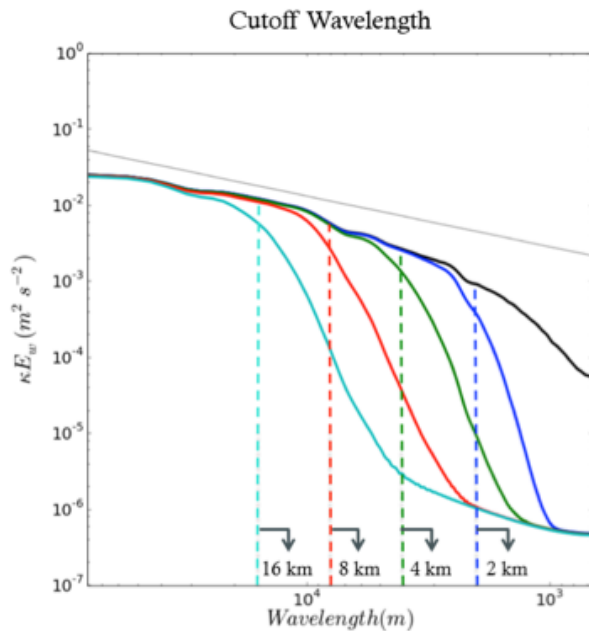

Figure 1. Spectra plot at time of initialization. Dashed lines indicate specified cutoff wavelength. Solid lines indicate energy when specified cutoff wavelength is applied. Black = raw simulation, blue = 2-km cutoff, green = 4-km cutoff, red = 8-km cutoff, and cyan = 16-km cutoff.

2. METHODS

2.1 *Model and experiment setup*

The simulations in this study are generated by the Advanced Research Weather Research and Forecasting Model (WRF-ARW; Skamarock et al. 2008; hereafter, "WRF") version 3.6.1, which is a three dimensional, nonhydrostatic, and fully compressible model (. The horizontal grid spacing is set to 333 m, and the model height is 20 km, with higher resolution towards the surface and coarser resolution as the model top is approached. The initial condition for the control run (hereafter, the "truth" or the "raw simulation") is unfiltered.

The initial conditions for the remaining simulations are generated by filtering the control simulation at prescribed times. We are implementing the implicit tangent filter of Raymond et al. (1988) to remove scales in the initial conditions smaller than specified wavelengths: 2, 4, 8, and 16 km. The effects of cutoff wavelength on the initial conditions are shown in Figure 1. The names of the filtered simulations contain a suffix indicating the cutoff wavelength, e.g., "_8km". In order to get a more general idea of the initial condition sensitivity, two different soundings for the idealized experiments are used: a sounding based on Weisman and Klemp 1982 (referred to as "WK82") and a Rapid Update Cycle (RUC; Potvin and Flora 2015) sounding near the 24 May 2011 supercell that produced an EF5 tornado in El Reno, OK ("El Reno"). The thermodynamic and wind profiles of both soundings are shown in Figure 2. We have multiple sets of simulations, where each set includes five runs using the same sounding: the control run, and the four variously filtered runs. The simulations are idealized (e.g., radiation and surface physics are neglected); more information pertaining to the model parameters of the idealized runs can be found in Table 1.
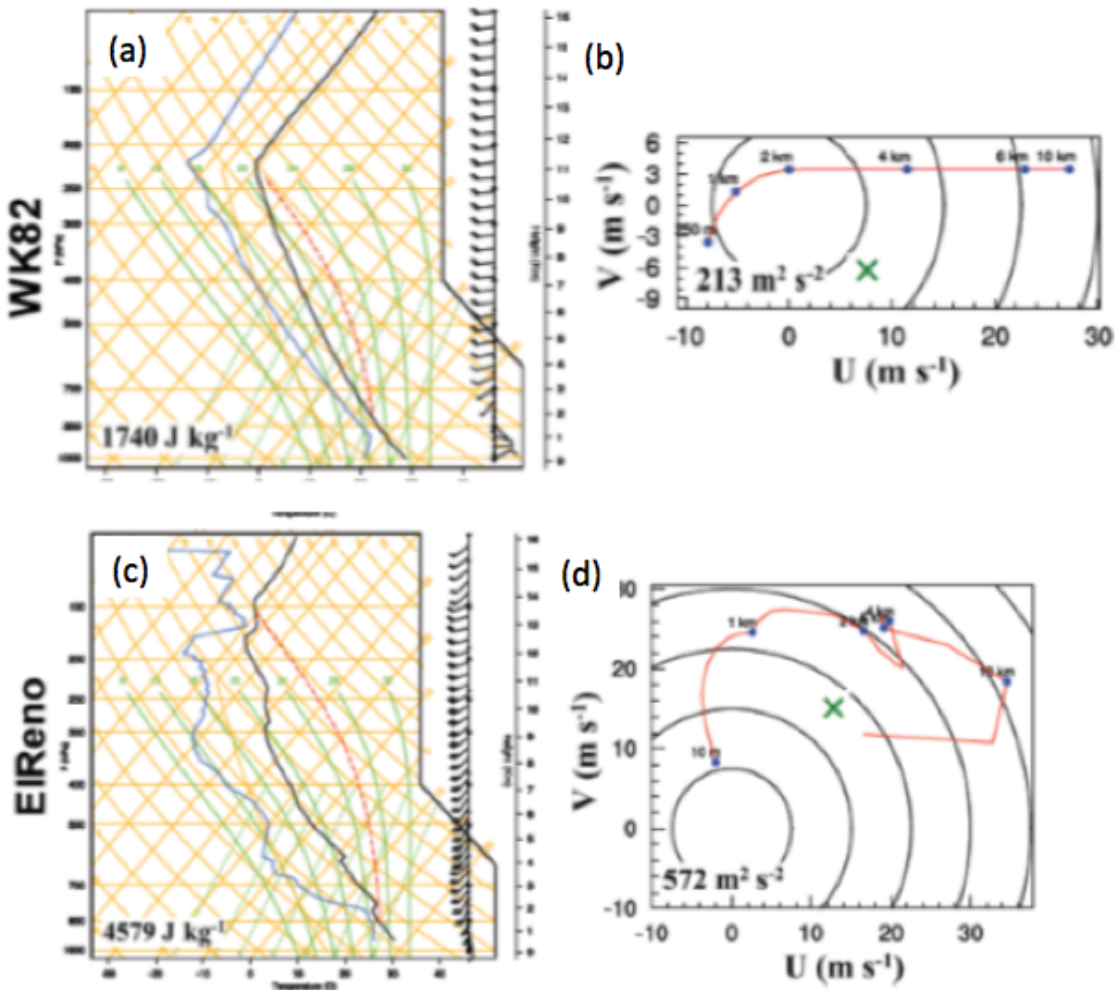
Figure 2. Skew-T soundings and corresponding hodographs used in (a, b) WK82 and (c, d) ElReno simulations. Surface-based convective available potential energy (CAPE) and 0-3 km AGL storm-relative helicity (SRH) are indicated on the Skew-T and hodograph plots, respectively. Mean storm motion vectors (used in SRH calculations and indicated by green "x"s on hodographs) were computed using the locations of the hook echo signatures at t = 30 min and t = 120 min.

Horizontal grid spacing	333 m
Vertical grid spacing	110 m < Δz < 550 m
Horizontal grid size	WK82: 661 × 661; ElReno: 901 × 901
Large / small time step	1 s / 1/6 s
Time-integration scheme	3rd-order Runge-Kutta
Horizontal / vertical advection	5th-order / 3rd-order
Lateral / top boundary conditions	Open / Rayleigh damping layer
Turbulence parameterization	1.5-order TKE closure
Microphysics parameterization	Thompson scheme
Coriolis effect	Off
Surface drag	Off
Radiation parameterization	Off
Cumulus parameterization	Off
Surface layer physics	Off
Planetary boundary layer parameterization	Off
Explicit numerical diffusion	Off
Horizontal / vertical bubble radii (control experiments only)	10 km / 1.5 km

Table 1. WRF-ARW 3.6.1 settings used in all experiments.

There are 3 sets of simulations initialized with the WK82 sounding. In the first set, the raw simulation is initialized with a thermal bubble, and the filtered simulations are initialized 30 minutes into the raw simulation; this set is referred to as the WK82_30min simulations. As will be furthered discussed in section 3, the WK82_30min_8km run produced a tornado-like vortex that was not present in the raw simulation. We therefore chose to use WK82_30min_8km, hereafter WK82-tor, as the control run for the next two sets of simulations. The filtered simulations in these two experiment sets were initialized at t=60 min (WK82-tor_60min) and t=90 min (WK82-tor_90min), where t is specified relative to the initialization time of the original WK82 control simulation to convey the degree of storm maturity at the beginning of each set of simulations.

The last set of simulations run in this study uses the El Reno sounding and an initialization time of 30 min for the filtered simulations. This experiment set is referred to as ElReno_30min. Figure 3 displays the naming conventions and initialization times for the filtered runs in each set of simulations in this study.

In order to determine if a simulation produced a tornado, different levels of the horizontal wind and vertical vorticity fields are examined at the time of a potential tornado, as shown in Figure 4. If significant rotation (rather than vorticity associated with linear shear) is present through the lowest 2 km, then this is classified as a tornado. If there is rotation at the surface at a particular time, but only for a brief period and/or with little vertical continuity, then this was considered a "quick spin up" and not a tornado.

2.2 *Plot setup*

Three of the types of plot used in this study warrant some explanation: time-height composites, horizontal composites, and power spectra. Time-height composites display the maximum value of a field over the entire horizontal domain as a function of time and height. One of the primary roles of these plots in this study is to diagnose the longevity and vertical continuity of strong low-level rotation (and thereby detect tornadoes) in the simulations. Horizontal composites show the maximum value of a field over the entire duration of the simulation. Power spectra plots show the amount of signal present within a field as a function of wavelength. We use these plots to compare the output of the filtered simulations to that of the control run to determine how quickly scales filtered from the initial condition are regenerated as the simulation proceeds.

3. RESULTS

We now describe the simulation analyses variable by variable.

3.1 *Reflectivity*

The reflectivity field at the time of initialization shows a steady degradation with increased cutoff wavelength, as expected (Figure 5). The WK82_30min_16km reflectivity field has lost much of the supercellular structure at initialization. However, the reflectivity differences at the end of the simulations would be insignificant from a forecaster's perspective. Thus, the reflectivity fields of the WK82_30min experiments show little
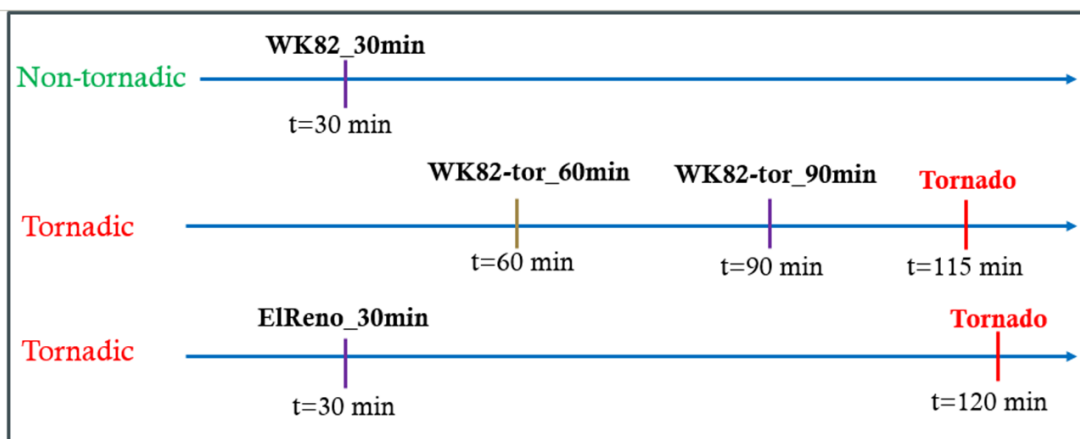
Figure 3. Initialization times for filtered runs in each set of experiments. Start times of tornadoes in tornadic simulations are shown.
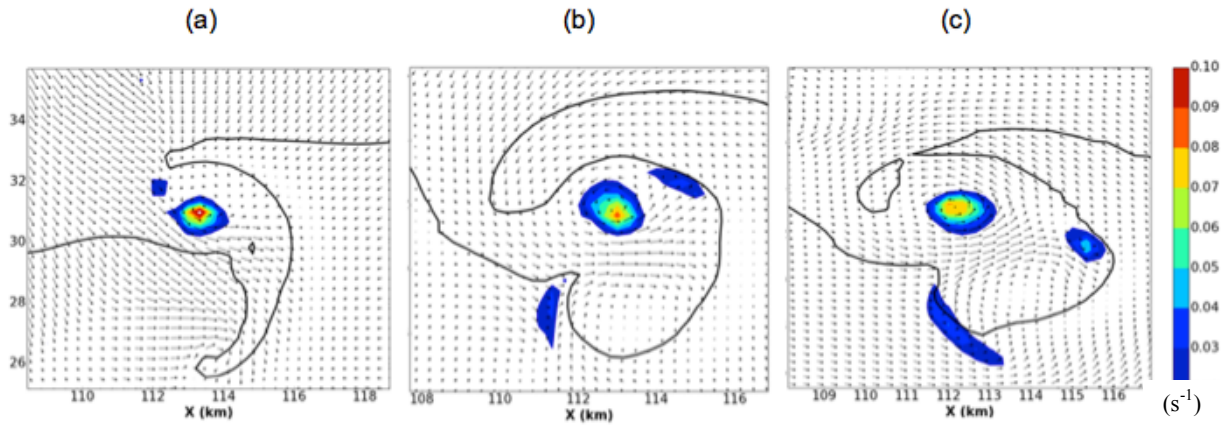
Figure 4. Horizontal cross-sections of vertical vorticity at (a) ~800 m, (b) ~2100 m and (c) ~3700 m.

sensitivity to the initial condition resolution. Similar results were obtained for the WK82_tor_60min, WK82-tor_90min, and ElReno_30min experiments. All the filtered simulations accurately forecast the track and orientation of the storm, including the placement of the areas with the highest dBZ and therefore significant hail potential. The relative insensitivity implies that reflectivity is primarily reliant on the larger-scale processes that are driving the storm at the initialization time, rather than on smaller-scale processes, whose omission would otherwise induce substantial forecast errors.

3.2 Vertical Velocity

Strong updraft velocities are indicative of a mature supercell capable of producing severe weather. This makes vertical velocity an operationally important model variable. Time-height composites of updraft speed reveal generally trivial differences among the WK82_30min experiments as shown in Figure 6. On the other hand, the WK82_30min_8km composite shows slightly overpredicted vertical velocities in several parts of the atmosphere, but most importantly in the lower 2 km. The WK82_30min_16km shows severely underpredicted vertical velocities within the first 10 minutes of the simulation, an error that recurs in other variables and experiments throughout this study. These delays arise because as larger scales are filtered out with increased cutoff wavelengths, the simulation takes more time to build these scales back, weakening some of the model fields in the beginning of the simulation. The WK82_30min_16km run also produces a relative maximum low-level updraft that extends to the surface and is not present in the control simulation. Such a false low-level updraft could mislead a forecaster about the tornado potential of a storm.
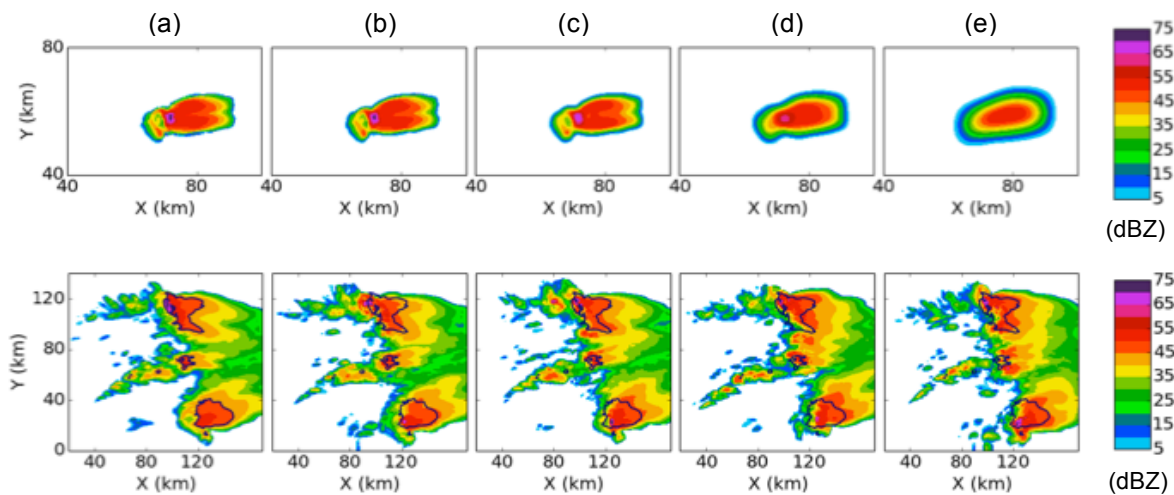

Figure 5. Top panels: the reflectivity field at initialization (t=30) for (a) WK82_30min control simulation, (b) 2 km cutoff, (c) 4 km cutoff, (d) 8 km cutoff and (e) 16 km cutoff. Bottom panels: as for top panels but valid 2 h into the simulation.
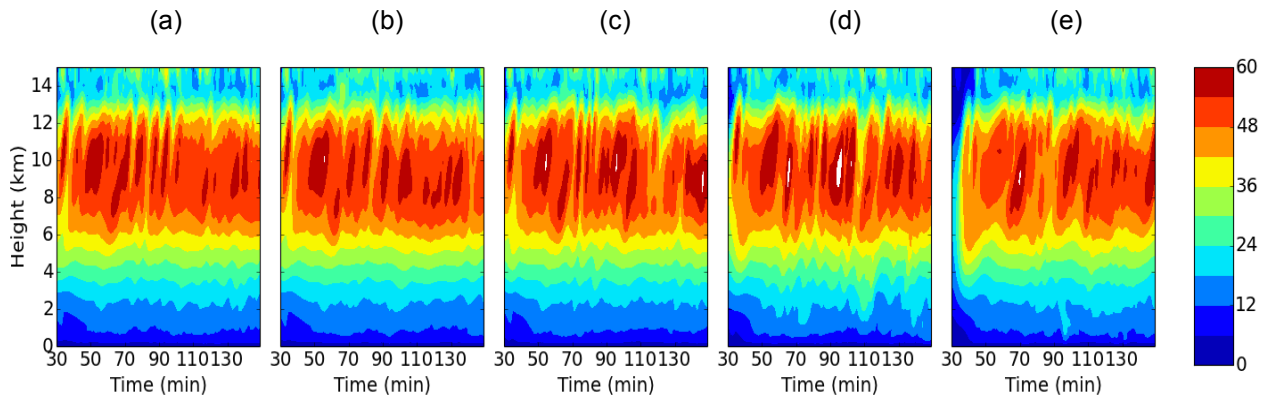
Figure 6. Vertical velocity (m/s) time-height composite for (a) WK82_30min control simulation, (b) WK82_30min_2 km, (c) WK82_30min_4 km, (d) WK82_30min _8 km, and (e) WK82_30min _16 km.
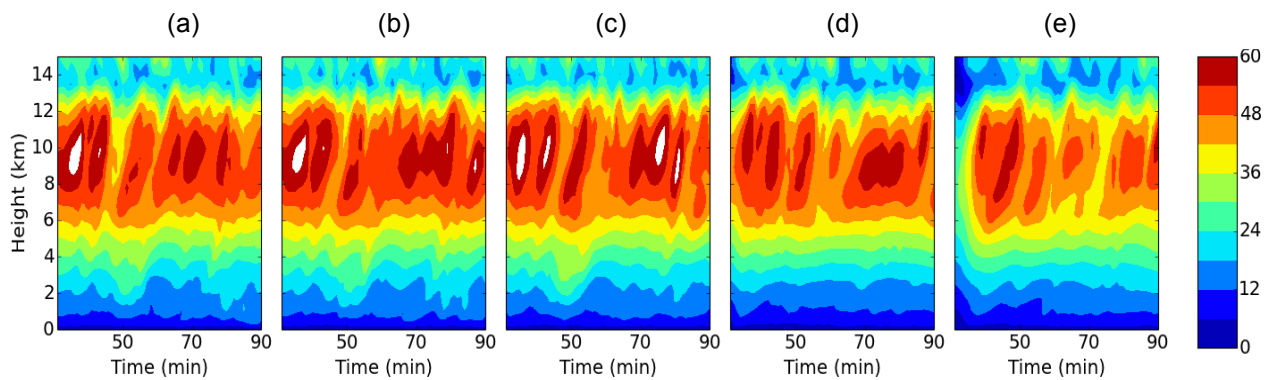

Figure 7. As in Fig. 6 but for WK82-tor_90min simulations.

The WK82-tor_60min and ElReno_30min experiments show only small deviations from the truth but with the 16 km simulations showing similar weakened vertical velocities during the first 10 minutes as in the WK82_30min experiments. However, the updrafts are generally accurately forecast throughout the simulations.

The WK82-tor_90min composites (Figure 7) show a monotonic degradation of the vertical velocities with increased levels of filtering, unlike the other sets of simulations, and displays the highest sensitivity. The WK82-tor_90min_8km and WK82-tor_90min_16km experiments lose temporal variation and have weaker amplitudes of relative maxima.

3.3 Vorticity

Vorticity is one of the most important model parameters to this study due to its implications for WoF; throughout this study, it is used as a proxy for tornado potential. The WK82_30min set (not shown) exhibits some variation in the vorticity

time-height composites, with the WK82_30min_4km and WK82_30min_16km simulations deviating most strongly from the control. They show near-surface, short-lived levels of vorticity, but with further analysis of the atmospheric state at those times, these vorticity maxima are classified as spin ups and not strong tornadoes. WK82_30min_8km, on the other hand, produces a tornado-like vortex that contains strong vorticity throughout the lower 4 km, which constitutes a false alarm in this case.

The ElReno_30min simulations (Figure 10) contain some significant differences, however, there is no obvious pattern to the errors. The control simulation contains a strong tornado-like vortex from t=120 to the end of the simulation. While the filtered simulations still produce strong vorticity maxima near the end of the simulation, the number, strength, and timing of the maxima are different for all runs with no distinguishable pattern.
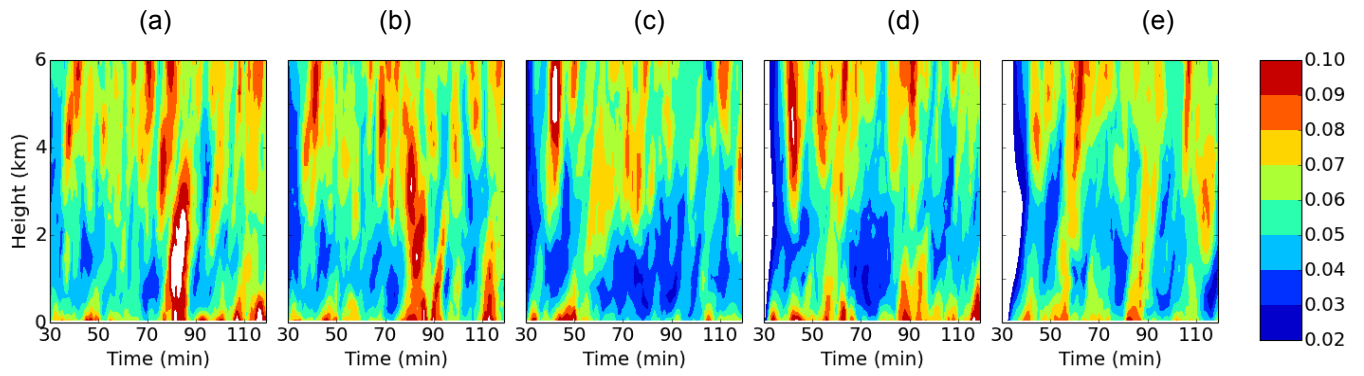
Figure 8. Vertical vorticity (s^{-1}) time-height composites for (a) WK82-tor_60min control simulation, (b) WK82-tor_60min_2 km, (c) WK82-tor_60min _4 km, (d) WK82-tor_60min _8 km, and (e) WK82-tor_60min _16 km.
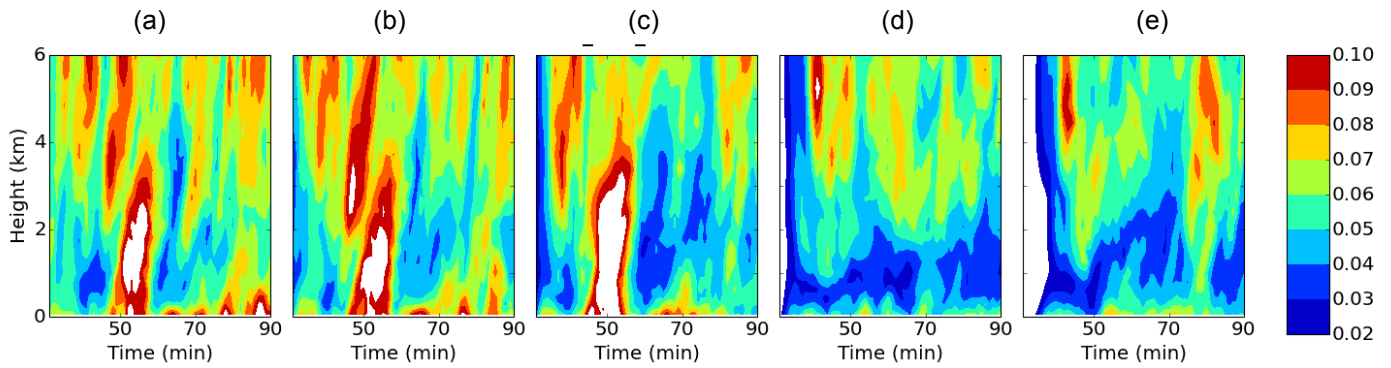

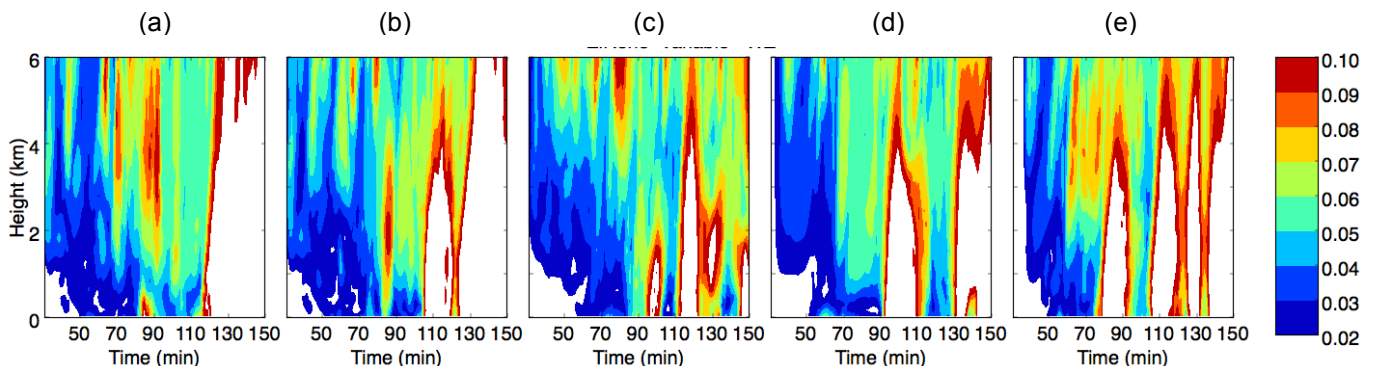Figure 9. As in Fig. 8 but for WK82-tor_90min simulations.

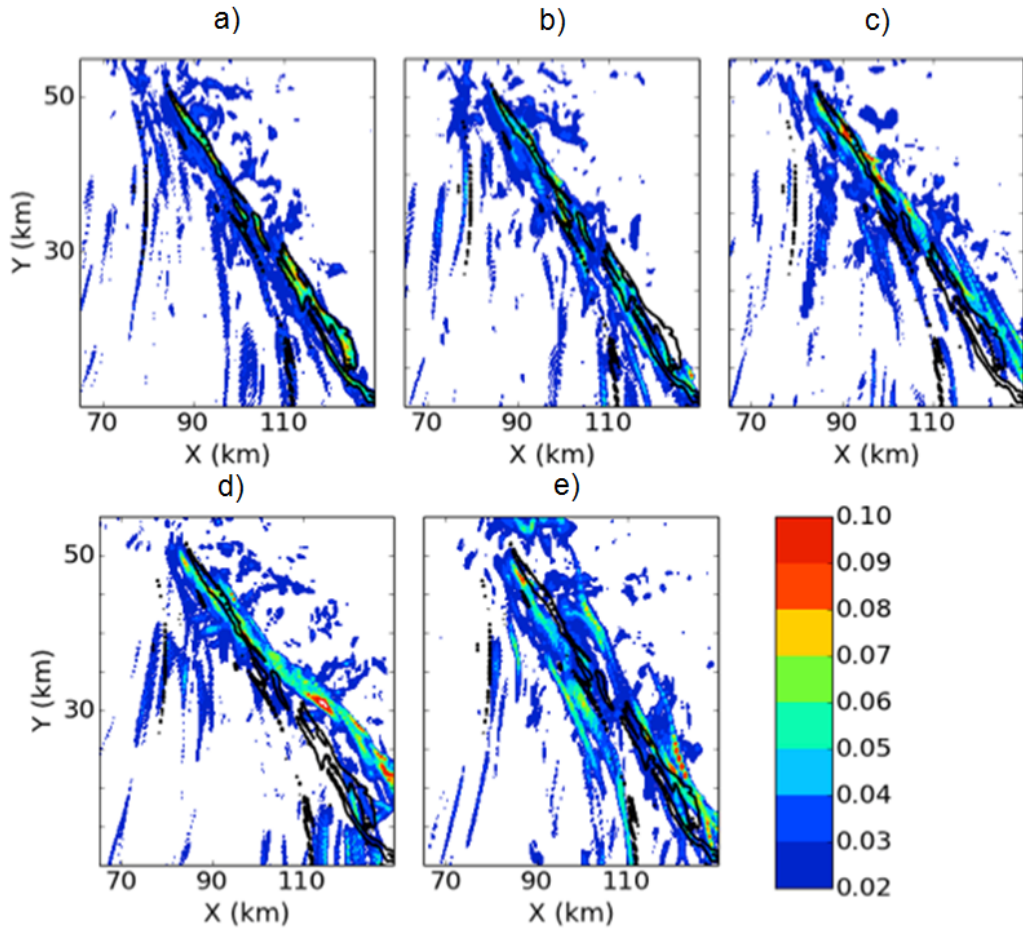Figure 10. As in Fig. 8 but for ElReno_30min simulations.

Figure 11. Horizontal vorticity (s^{-1}) composites for (a) WK82_30min control simulation, (b) WK82_30min_2 km, (c) WK82_30min _4 km, (d) WK82_30min _8 km, and (e) WK82_30min _16 km.

We generate horizontal composites showing the maximum vorticity below 2 km AGL over the duration of the simulation. These illustrate the track and strength of the low-level rotation. The previously noted tornado false alarm in WK82_30min_8km is again apparent here (Figure 11). The WK82_30min_16km does not show a well-defined track of maximum vorticity, but it does not produce a relative maximum like the WK82_30min_8km.

The WK82-tor_60min set, similar to the WK82_30min set, shows no obvious pattern with increasing cutoff wavelength, with the WK82-tor_60min_4km simulation producing the worst forecast (not shown). However, the WK82-tor_90min set produces a monotonic degradation with increasing cutoff wavelength (Figure 12), which is consistent with previous analysis of this experiment. The maximum vorticity track is forecasted more accurately in the ElReno_30min experiments than in the WK82 simulations; however, the sensitivity of vorticity amplitude and timing previously seen in the time-height composites (Figure 10) is also evident in the horizontal composites (Figure 13). For example, the premature onset of intense low-level vorticity in the 8- and 16-km simulations is evident. Thus, operationally significant vorticity forecast errors occur in all of the experiments.
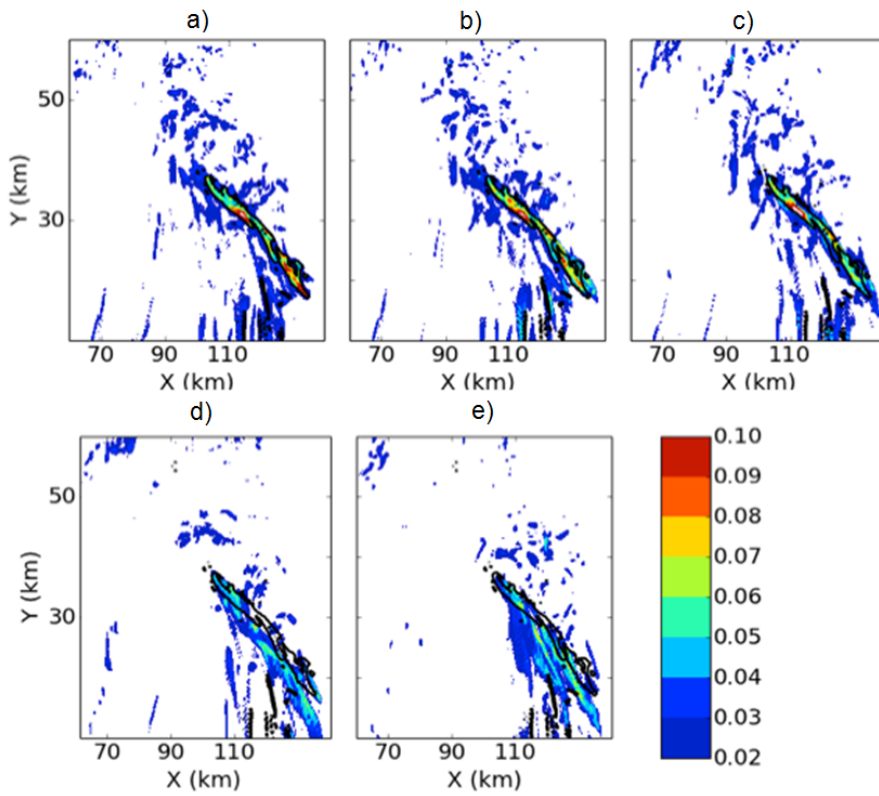
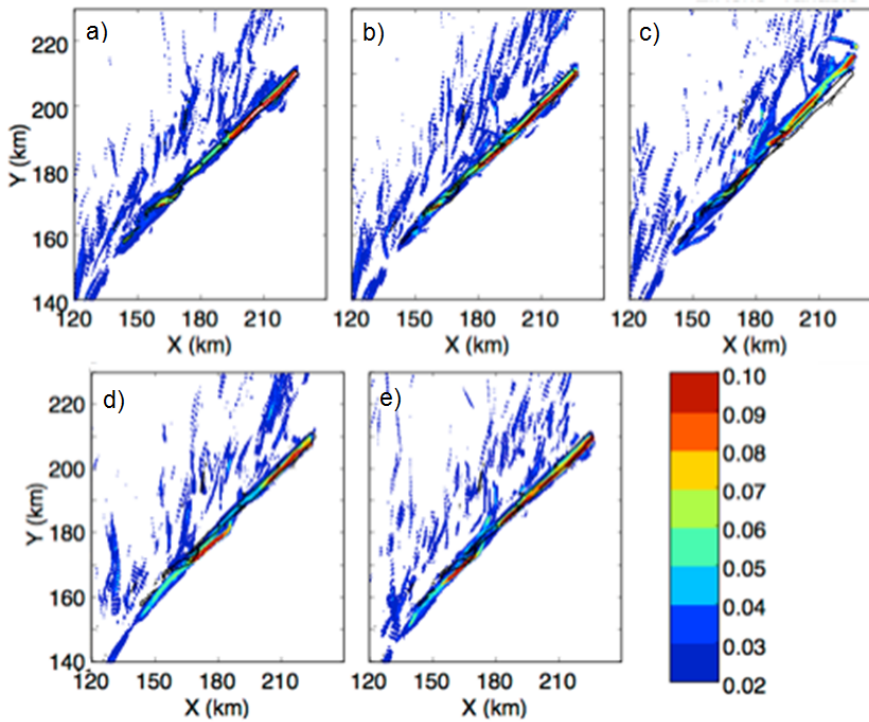Figure 12. As in Fig. 11 but for WK82-tor_90min simulations.

Figure 13. As in Fig. 11 but for ElReno_30min simulations.

3.4 Rainfall

Horizontal composites of total rainfall are useful for predicting areas of potential flooding. All WK82 and ElReno experiments show limited sensitivity of rainfall to initial condition resolution. The placement of the highest amounts of rainfall is fairly accurate with no steady pattern to the error with increased cutoff wavelengths. However, the amplitudes of the maxima in some of the simulations vary as seen in Figure 14 for the WK82_30min experiments. The WK82_30min_16km simulation shows the maximum to be an inch less than what the truth simulation produces. While this is a large amount of rainfall, the simulations are still accurate enough to give a forecaster the information necessary to predict the areas with the highest flooding potential.

3.5 Surface wind speed

The maximum surface wind speed can be used as an estimate for the damaging straight-line wind potential in a storm. Figure 15 shows results that are representative of all the WK82 and ElReno experiment sets. As with rainfall, the filtered simulations correctly predict the approximate locations at greatest risk for damaging winds. Maximum surface wind time series (not shown) revealed substantial errors in the 8-km and 16-km simulations during the first 10 minutes. We attributed these errors to the fact that scales that are filtered from the initial condition require time to regenerate in the model, as we've previously seen.

3.6 Spectra

The spectra of four different variables are analyzed for all simulations in this study: temperature, vertical velocity, horizontal velocity, and rainwater mixing ratio (q_r). The filtered scales in all four variables largely regenerate within the first 20 minutes of the simulations, even for the 16-km experiments (Figure 16). Temperature is the quickest parameter to fully regenerate. Vertical velocity recovers quickly as well, though the 16 km simulations have not totally recovered after 20 minutes. This is more evident in spectra ratio plots (Figure 17), which highlight small differences between each filtered run and the control simulation. Horizontal velocity spectra follow similar patterns as the vertical velocities, as
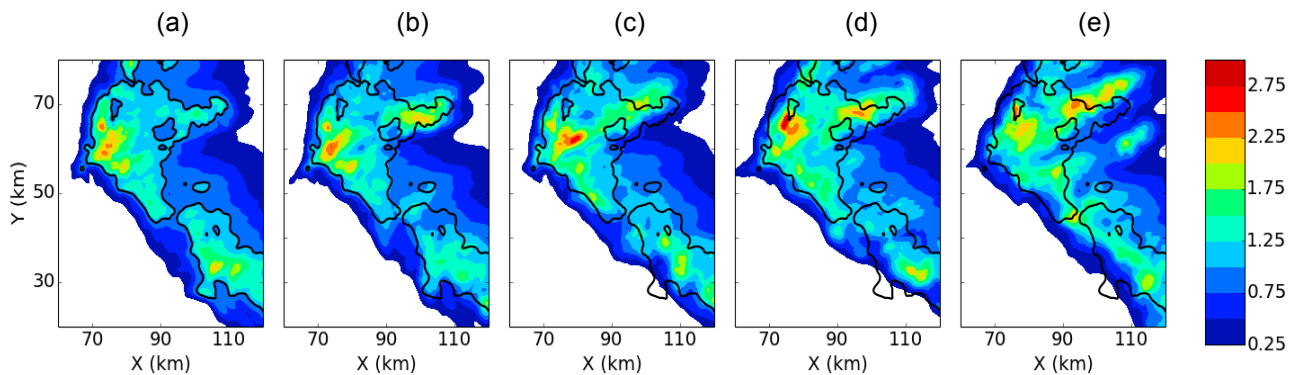

(a)   (b)   (c)   (d)   (e)

Figure 14. Horizontal composites of accumulated rainfall (in) for (a) WK82_30min control simulation, (b) WK82_30min_2 km, (c) WK82_30min _4 km, (d) WK82_30min _8 km, and (e) WK82_30min _16 km.

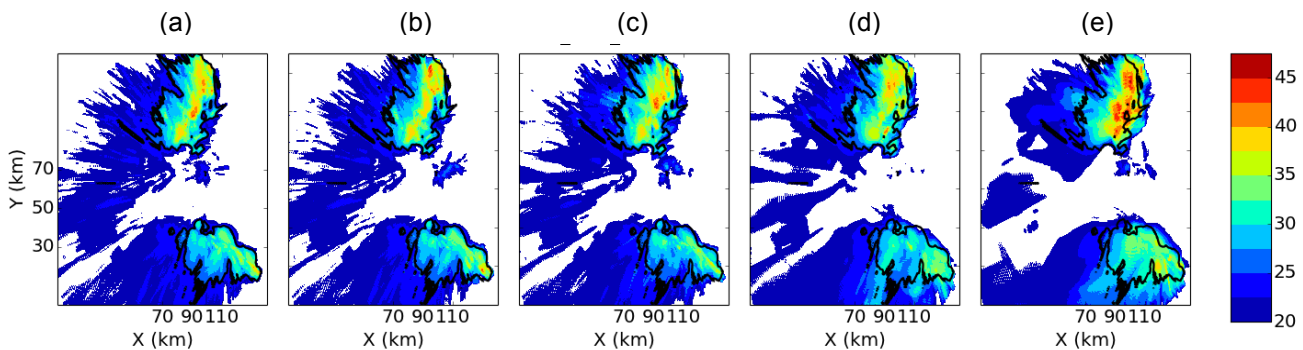(a)   (b)   (c)   (d)   (e)

Figure 15. Horizontal composites of maximum surface wind speed (m/s) for (a) WK82-tor_90min control simulation, (b) WK82-tor_90min_2 km, (c) WK82-tor_90min _4 km, (d) WK82-tor_90min _8 km, and (e) WK82-tor_90min _16 km.

expected (not shown). Spectra of q_r vary slightly more than the other parameters examined (not shown). In the WK82_30min, WK82-tor_60min and ElReno_30min sets of simulations, the q_r spectra ratios fluctuate during the first 20 minutes. However, q_r still recovers quickly enough to produce accurate rainfall forecasts. In summary, for all four variables examined, the filtered scales generally recover rapidly, consistent with the relative insensitivity of the simulations to initial condition resolution (with the notable exception of low-level vorticity).

4. DISCUSSION

As shown in this study, scales that are initially missing in supercell simulations regenerate quickly, generally within the first 10-20 minutes. Once these scales are rebuilt, the model is able to produce a forecast that largely resembles the control simulation ("truth"), even when wavelengths up to 16 km are filtered from the initial condition. This was true for most of the model parameters examined: reflectivity, updraft strength, rainfall, and surface wind speeds. Thus, forecasts that are initialized by downscaling relatively coarse data assimilation analyses may have considerable value for severe storm operations. This is encouraging given that current computational and observational limitations preclude performing data assimilation at arbitrarily fine resolution.

Low-level vorticity, however, was found to be much more sensitive to the initial condition resolution. Operationally significant errors occurred in many of the simulations with cutoff wavelengths ≥ 4 km. Since current NWP models poorly resolve wavelengths < $4\Delta x$, where Δx is the horizontal grid spacing, these results suggest that accurate data assimilation on 1-km model grids is required for reliable prediction of intense low-level vorticity (and therefore tornadoes).

Of the four sets of experiments performed herein, the WK82-tor_90min simulations are the only ones that were initialized during a mature stage of the storm, and are also the only simulations that show a monotonic degradation of vertical velocity and vorticity with increasing initial condition filtering. Furthermore, these simulations exhibit greater initial condition resolution sensitivity than the other WK82 simulations. We hypothesize that these differences in behavior arise from the increasing importance of smaller-scale processes as the storm matures. Early in the simulations initialized at t=30 min or t=60 min, larger-scale processes are primarily driving the storm, allowing

time for the smaller scales removed from the system to regenerate before they begin playing a greater role in the storm evolution. Conversely, the simulations initialized at t=90 min contain a mature storm that is now more driven by smaller-scale processes that therefore do not have time to build back before their absence impacts the subsequent storm evolution, thus degrading the forecast. Thus, errors arising from limited initial condition resolution may sometimes *increase* as forecast lead-time decreases.

The work presented herein is preliminary and could be greatly expanded. In order to further illuminate the initial condition resolution sensitivities of supercells and their implications for Warn-on-Forecast, we will conduct additional ElReno experiments initialized later in the storm life cycle (closer in time to the tornado-like vortex in "truth"). We will also perform full-physics simulations that better replicate real storm processes and current NWP models. The results of this work will help guide the design of future Warn-on-Forecast ensemble systems
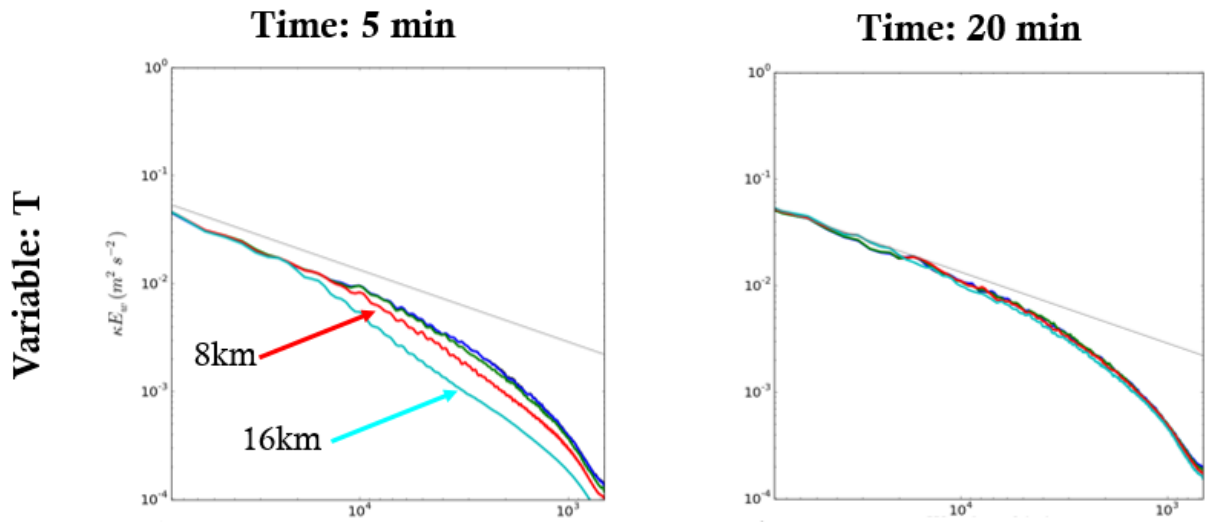
Figure 16. Spectra plots of temperature in the WK82-tor_60min experiments, with WK82-tor_60min_8km and WK82-tor_60min_16km highlighted. Times are relative to the initialization of the filtered simulations.
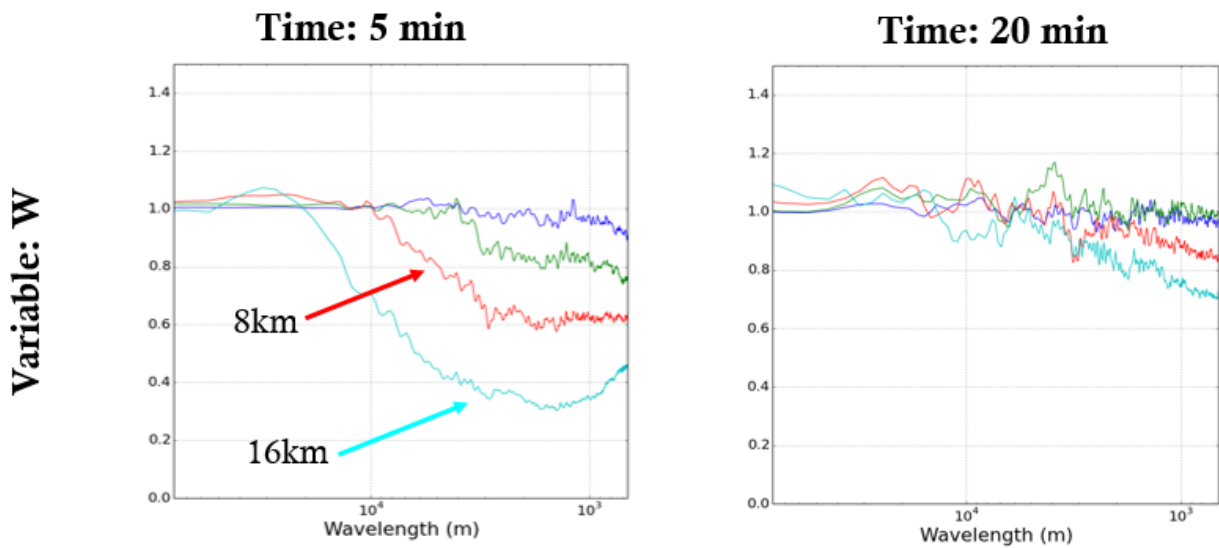

Figure 17. As in Fig. 16 but for vertical velocity.

6. REFERENCES

Davies-Jones, R., 2015: A review of supercell and tornado dynamics. *Atmospheric Research*., **158-159,** 274-291.

Lemon L.R., and C.A., Doswell III, 1979: Severe Thunderstorm Evolution and Mesocyclone Structure as Related to Tornadogenesis. *Mon. Wea. Rev.*, **107**, 1184–1197.

Markowski, P.M., and Y.P., Richardson, 2009: Tornadogenesis: Our current understanding, forecasting considerations, and questions to guide future research. *Atmospheric Research*., **93**, 3-10.

Potvin, C. K., and M.L. Flora, 2015: Sensitivity of idealized supercell simulations to horizontal grid spacing: Implications for Warn-on-Forecast. *Mon. Wea. Rev.*, in press.

Raymond, W. H., 1988: High-order low-pass implicit tangent filters for use in finite area calculations. *Mon. Wea. Rev.*, **116**, 2132–2141.

Skamarock, W.C., 2004: Evaluating mesoscale NWP models using kinetic energy spectra. *Mon. Wea. Rev.*, **132,** 3019-3032.

—, and Coauthers, 2008: A Description of the Advanced Research WRF version 3. NCAR Tech. Note NCAR/TN-475+STR,113pp.

Stensrud, D. J., Wicker, L. J., Xue, M., Dawson II, D.T., Yussouf, N., Wheatley, D.M., Thompson, T.E., Snook, N.A., Smith, T.M., Jung, Y., Jones, T.A., Gao, J., Coniglio, M.C., Brooks, H.E., Brewster, K.A., 2013: Progress and challenges with Warn-on-Forecast. *Atmospheric Research*., **123**, 2-16.

Stensrud, D.J., Xue, M., Wicker, L.J., Kelleher, K.E., Foster, M.P., Schaefer, J.T., Schneider, R.S., Benjamin, S.G., Weygandt, S.S., Ferree, J.T., Tuell, J.P., 2009: Convective-scale warn on forecast: a vision for 2020, *Bull. Amer. Meteor. Soc.,* **90**, 1487 – 1499.